

Multitemplate Alignment Method for the Development of a Reliable 3D-QSAR Model for the Analysis of MMP3 Inhibitors

Tiziano Tuccinardi,^{*,†,‡} Gabriella Ortore,[†] M. Amélia Santos,[§] Sérgio M. Marques,[§] Elisa Nuti,[†] Armando Rossello,[†] and Adriano Martinelli[†]

Dipartimento di Scienze Farmaceutiche, Università di Pisa, via Bonanno 6, 56126 Pisa, Italy, Sbarro Institute for Cancer Research and Molecular Medicine, Center for Biotechnology, College of Science and Technology, Temple University, Philadelphia, Pennsylvania 19122, and Centro de Química Estrutural, Instituto Superior Técnico, Rua Rovisco Pais 1, 1049-001 Lisboa, Portugal

Received March 31, 2009

A ligand-based 3D-QSAR study for the identification of MMP3 inhibitors was developed by applying an innovative alignment method capable of taking into account information obtained from available X-ray MMP3 structures. Comparison of the obtained model with data recently published using a docking-based alignment method indicated that the ligand-based 3D-QSAR model provided better predictive ability. A second external test set of 106 MMP3 inhibitors further confirmed the predictive ability of the 3D-QSAR model. Finally, certain iminodiacetyl-based hydroxamate-benzenesulfonamide conjugates, which were predicted to be active by the 3D-QSAR model, were tested *in vitro* for MMP3 inhibition; some provided low nanomolar activity. As such, our results suggest that the multitemplate alignment method is capable of improving the quality of 3D-QSAR models and therefore could be applied to the study of other systems. Furthermore, since MMP3 is an important target toward the treatment of arthritis, this model could be applied to the design of new active MMP3 inhibitors.

INTRODUCTION

Three-dimensional quantitative structure–activity relationships (3D-QSAR) involve the analysis of the quantitative relationship between the observed biological activity of a set of compounds and their three-dimensional properties using statistical correlation methods.

It is well-known that one of the main drawbacks of 3D-QSAR methods is the difficulty of obtaining suitable ligand alignments, which are so important that they affect the success of a model.

Many alignments methods have been reported in literature; among them in the last years the most used have been the cocrystallized conformer-based alignment (CCBA), the docking-based alignment (DBA), and the pharmacophore-based alignment (PBA).

The CCBA method is usually applied in the presence of compounds characterized by relative conformational rigidity. It starts from a crystallographic bound compound that is used as a starting geometry to construct the remaining compounds included in the study. Many 3D-QSAR studies have been reported using this alignment method.^{1–4} For example, Pandey and Saxena using 65 inhibitors of protein tyrosine phosphatase 1B reported the comparison of 3D-QSAR results obtained using the CCBA, the DBA, and the global minima energy conformer-based alignment, and, among the 3D QSAR models developed using the above three alignments, the CCBA provided the best results.¹

In the DBA methods the three-dimensional structure of a target protein, along with a docking protocol, is used as an alignment tool. In the last years this approach has been the most used, mainly because of the possibility of combining the accuracy of a receptor-based alignment with the computational efficiency of a ligand-based method. Furthermore, since the alignment is performed using structures docked into a three-dimensional structure of a target protein, the maps produced by the 3D-QSAR analysis can be compared with the neighboring amino acid residues surrounding the active site. Such an approach is thought to be a more rational way to develop new biologically active compounds since it is also possible to collect quantitative information from the contour maps generated by 3D-QSAR approaches. Several studies have been published in which the combination of docking-based methods and 3D-QSAR was successfully applied for the design and prediction of bioactive compounds, using experimentally determined three-dimensional structures^{1,5–11} or computational models^{12,13} of the target proteins.

In the PBA approach the essential features of one or more compounds generally characterized by a high activity are used for the alignment of the whole training and test sets. The pharmacophore model can be generated by means of a fully ligand-based approach^{14–17} or by the support of structural information derived from the target protein that, by means of docking or analysis of the available X-ray structures, can suggest the main protein–ligand interactions important for the activity.¹⁸

In the present paper we exploited the possibility of developing a 3D-QSAR model using a multitemplate alignment (MTA) approach. At the present time, the Protein Data Bank receives approximately 25 new experimentally deter-

* Corresponding author phone: +39(0)502219595; fax: +39(0)502219605; e-mail: tuccinardi@farm.unipi.it.

[†] Università di Pisa.

[‡] Temple University.

[§] Centro de Química Estrutural, Instituto Superior Técnico.

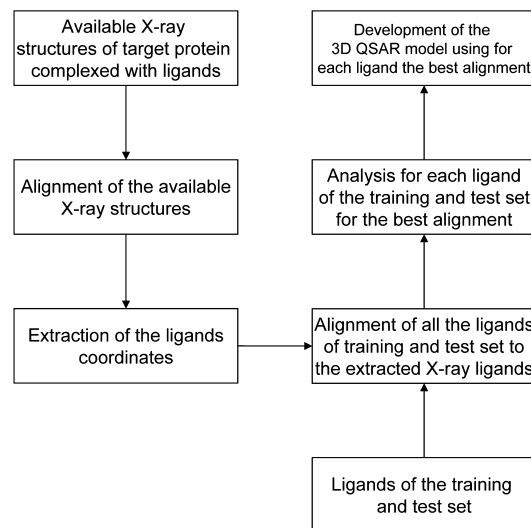


Figure 1. Schematic diagram of the multitemplate alignment method.

mined structures from scientists each day for inclusion in the archive. This archive now contains more than 56,000 current experimental structures, and it is estimated that the size of the PDB archive will triple to 150,000 structures by year 2014.¹⁹ For many proteins more than twenty X-ray complexes have already been deposited in the PDB archive, and for targets like carbonic anhydrase II or cyclin-dependent kinase 2 more than 50 experimentally determined protein–ligand complexes are available. In light of these data we tested the possibility of using all the available experimentally determined 3D structures of a target protein for developing an alignment method.

Figure 1 described the main steps of the proposed MTA procedure.

First the available X-ray structures of the target protein complexed with ligands were aligned with each other on the basis of protein sequence, and then the so aligned ligands were extracted from the complexes. After all the ligands belonging to the training and test set were then aligned to all the extracted ligands, for each ligand the alignment with the best score was taken into account. Finally using for each ligand of the training and test set this best alignment a 3D-QSAR model was developed.

In order to test this alignment approach the stromelysin (MMP3) was studied as a case study. We chose this target for several main reasons. First of all a good number of complexes between MMP3 and inhibitors have been deposited in the protein data bank. Furthermore we recently tested the ability of Gold software to predict the binding disposition of MMP inhibitors.⁹ The best procedure was subsequently employed to dock into MMP2, MMP3, and MMP9 nearly 70 compounds tested for their inhibitory activity against these three MMP subtypes, and the best binding poses were used as an alignment tool for the development of 3D-QSAR models. Therefore, using the same training and test set, the development of a MTA 3D-QSAR for this target could be compared to the results obtained using a DBA approach.

Finally, MMP3 is an important therapeutical target since this enzyme has a broad activity profile for macromolecular substrates including proteoglycan, and it is involved in a cascade of proteolytic activation of other members of the family. High levels of MMP3 are found in the synovial fluid

Table 1. Ligand Structures of the MMP3 X-ray Complexes Used in the Present Study

PDB Code	Ligand	PDB Code	Ligand
1B3D		1BIW	
1BQO		1D5J	
1D7X		1D8F	
1D8M		1G49	
2D10			

and cartilage of rheumatoid and osteoarthritis patients.²⁰ Therefore, selective inhibitors of MMP3 are required for the treatment of arthritic diseases, in order to slow down the progressive loss of cartilage,²¹ and the results obtained by this MTA 3D-QSAR model could be applied to the design of new active MMP3 inhibitors.

RESULTS AND DISCUSSION

Table 1 shows the nine published X-ray structures of MMP3 complexed with hydroxamic inhibitors that were considered in the current study.^{22–30}

These complexes were superimposed using 1B3D²² as a reference structure, and the ligands were then extracted and used as references molecules for the alignment. The 69 MMP3 inhibitors^{31–38} that had been previously used for the development of a docking-based 3D-QSAR for MMP2, MMP3, and MMP9, all bearing hydroxamate functionalities as ZBGs, were used as a training set (54 compounds) and an external test set (15 compounds). To this end, these

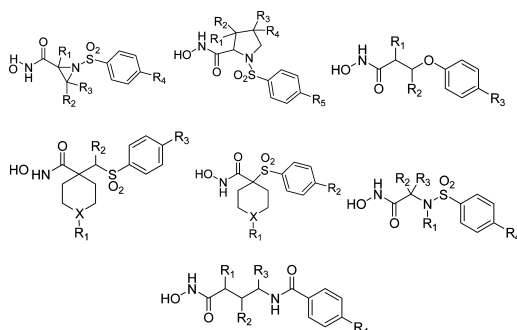


Figure 2. General scaffolds of the compounds used for the development of the 3D-QSAR model.

compounds were characterized by seven different central scaffolds (Figure 2), and they displayed inhibitory activities that spanned 5 orders of magnitude, with IC_{50} values ranging from 0.3 nM to 16 μ M.

These 69 compounds were aligned in turn with the nine reference molecules extracted from the X-ray complexes through OMEGA and ROCS programs.³⁹ OMEGA takes into account the flexibility of a molecule by generating all representative conformers, while ROCS compares the shapes of the molecules using a smooth Gaussian function. Using this software, each of the 69 MMP3 inhibitors was superimposed onto each of the nine X-ray ligands (see Figure 3), and scores were obtained measuring the quality of the superimposition. Therefore, for each of the 69 inhibitors nine possible scored alignments were generated.

The alignment of all available experimental structures of MMPs complexed with ligands containing a hydroxamate functional group such as zinc binding group (ZBG) suggested that the hydroxamate interacts with the zinc ion in the same binding position for all MMPs. As such, a good superimposition of the hydroxamate group of the MMP3 inhibitors onto those of the X-ray ligands was considered as a prerequisite for assessing the validity of the superimposition. To this end, the root-mean-square deviation (rmsd) between the hydroxamate ZBG of the reference ligands and that of the MMP3 inhibitors was measured, and, among the nine superimpositions studied, only those in which the rmsd between the ZBG of the inhibitor and that of the reference ligand was lower than 1.2 Å were retained and, among these, the one showing the higher alignment score was selected. For inhibitors that did not display any rmsd for the ZBG below 1.2 Å, the superimposition with the lowest ZBG rmsd value was selected.

In conclusion, a single superimposition was taken into account for each ligand, and these superimpositions defined the alignment for the development of the ligand-based 3D-QSAR. In order to compare the results with those recently obtained for the docking-based 3D-QSAR,⁹ the model was developed using the GRID/GOLPE approach using the C3 and N2 probes, following a previously reported procedure.⁹

Table 2 lists the primary data for the 3D-QSAR analysis. The first partial least-squares (PLS) component explained 86% of variance and was predictive ($q^2 = 0.66$, standard deviation of errors of prediction (SDEP_{TSI}) of the test set = 0.73), and the second PLS component improved both the fitting and the predictive ability of the model ($r^2 = 0.91$, $q^2 = 0.77$, and the SDEP_{TSI} of the test sets = 0.64), while the third PLS component provided no further improvement in

predictivity. Thus, the model's optimal dimensionality was given by two components (see Figure 4 and Table 2).

These results provided, in terms of predictive ability, an improvement over the previously reported DBA 3D-QSAR model, even if for two compounds of the test set (**19** and **36**) the predicted activity differed from the experimental activity more than one logarithmic unit. As shown in Table 3 the DBA 3D-QSAR model showed an r^2 and q^2 of 0.91 and 0.77, respectively, which were similar to those reported for the MTA 3D-QSAR model; however, the DBA 3D-QSAR model displayed poorer predictive ability overall, as it showed a higher SDEP of the external test set (SDEP_{TSI} = 0.79) with respect to the one obtained from the MTA model (SDEP_{TSI} = 0.64).

One important feature of 3D-QSAR analysis is the graphical model representation, which is used to make interpretation more straightforward. In the GOLPE program,⁴⁰ there are several options for displaying the final model. Among these, the PLS pseudocoeficient plots are very useful since they make it possible to visualize favorable and unfavorable interactions between the probes and the molecules under study. Figure 5 illustrates the PLS coefficient plots of the model for the C3 and N2 probes. Compound **67** (see Table 4) is also reported. The left part of Figure 5 shows the positive (green polyhedrons) and negative (cyan polyhedrons) PLS coefficients for the C3 probe. Notably, there are four principal regions (A-D) with positive values, in which a favorable interaction between a substituent and the probe determines an increase in activity, while an unfavorable interaction between a substituent and the probe determines a decrease in activity. The negative PLS coefficients indicate areas where a favorable interaction between a substituent and the probe determines a decrease in activity, while an unfavorable interaction between a substituent and the probe determines an increase in activity. In this picture, two regions (A' and B') are observed. The right part of Figure 5 reports the positive (green polyhedrons) and negative (cyan polyhedrons) PLS coefficients for the N2 probe. There are two regions (a' and b') with negative values, in which a favorable interaction between a substituent and the probe determines an increase in affinity, while an unfavorable interaction between a substituent and the probe determines a decrease in affinity. There are five positive regions (a-e) where a favorable interaction between a substituent and the probe determines a decrease in affinity. Regions a, d, and e correspond to the A, B, and D regions of the C3 probe, suggesting an important lipophilic role for these three lipophilic regions.

Figure 6 illustrates the PLS coefficient for the C3 and N2 probes as a triangle mesh and compounds **67**, **63**, **12**, and **27** (see Table 4) embedded in their positive activity contribution plots, displayed as red polyhedrons. While the PLS coefficient plots provide a global interpretation of the 3D-QSAR model, the activity contribution plots allow for the display of spatial regions that are individually important for the selected molecules.

The phenylmethylsulfane substituent of compound **67** (MMP3 $IC_{50} = 3.0$ nM) favorably interacted with regions C and D of the C3 probe, and the 3,3-dimethylpyrrolidine ring favorably interacted with region B. The interaction with regions d and e of the N2 probe confirmed the importance of the aforementioned lipophilic interaction of the phenyl

PROTEIN												
	1B3D		1BIW		1BQO		1D5J		1D7X		1D8F	
LIGANDS	CSCORE	ZBG	CSCORE	ZBG	CSCORE	ZBG	CSCORE	ZBG	CSCORE	ZBG	CSCORE	ZBG
1	0.9	2.1	0.8	1.5	0.8	9.0	0.9	3.0	1.0	6.3	0.9	> 10
2	1.3	0.9	0.8	1.4	0.8	7.1	1.1	0.8	1.1	0.8	0.9	6.3
3	1.4	0.9	0.8	1.4	0.9	1.1	1.1	0.7	1.1	0.7	1.0	0.6
4	1.0	5.9	0.8	1.4	0.8	7.2	1.0	4.5	0.9	6.8	0.9	9.6
5	1.0	5.8	0.8	5.1	0.8	4.2	1.0	4.1	0.9	5.3	0.9	9.5
6	0.9	0.8	0.7	1.5	0.8	6.0	0.9	4.1	0.9	5.9	0.8	6.2
7	1.0	4.5	0.7	1.5	0.8	6.0	1.0	4.6	1.0	5.3	0.9	6.2
8	0.9	3.8	0.7	1.5	0.8	6.0	0.9	4.1	0.9	4.7	0.9	4.5
9	0.9	0.8	0.7	1.5	0.8	5.7	0.9	4.1	0.9	5.9	0.9	5.4
10	1.3	0.9	0.8	1.4	0.9	1.1	1.2	1.0	1.1	0.7	1.1	0.6
11	1.1	0.8	0.7	1.9	1.0	1.0	1.0	0.7	1.0	0.6	0.9	1.1
12	1.2	0.9	0.8	5.8	1.0	1.1	1.0	0.7	1.0	0.8	1.0	0.7
13	1.2	0.8	0.8	1.5	0.8	3.4	1.1	0.7	1.1	0.6	1.0	0.5
14	0.9	6.3	0.8	1.4	0.9	6.1	0.8	4.0	0.9	7.4	0.9	6.3
15	1.0	6.3	0.8	1.4	0.8	7.1	0.9	4.7	1.0	5.3	0.9	5.5
16	1.2	0.7	0.8	> 10	0.9	4.5	1.1	0.7	1.0	0.6	1.1	0.6
17	0.9	6.3	0.8	1.2	0.8	5.4	1.0	5.6	1.0	4.6	0.9	10.0
18	1.2	0.9	0.8	1.8	0.8	3.8	1.2	0.8	1.2	0.7	1.0	6.4
19	1.2	0.8	0.8	5.3	0.8	6.0	1.2	0.6	1.2	0.7	1.0	5.4
20	1.4	0.9	0.8	1.4	0.8	5.4	1.1	0.7	1.1	0.7	1.1	0.6
21	1.3	0.9	0.8	> 10	0.9	1.1	1.1	0.7	1.1	0.7	1.0	0.6
22	1.4	0.9	0.8	1.1	1.0	1.1	1.2	0.7	1.2	0.8	1.1	0.6
23	0.9	1.0	0.7	0.6	0.8	5.6	0.9	0.6	0.9	5.0	1.1	6.6
24	0.9	1.5	0.7	3.7	1.0	5.4	0.9	4.3	1.1	0.6	1.2	7.9
25	0.9	1.6	0.8	0.6	1.0	5.4	1.1	0.4	1.2	0.6	1.2	7.8
26	0.9	3.3	0.8	4.2	0.7	7.0	0.8	> 10	1.0	5.4	1.0	5.7
27	1.0	0.9	0.8	0.6	0.9	5.2	1.1	0.4	1.2	0.6	1.0	7.9
28	0.9	3.2	0.8	5.1	0.7	7.4	0.8	4.3	1.0	5.3	1.0	5.7
29	1.1	5.8	0.8	0.3	0.9	1.2	0.9	0.9	1.0	0.6	0.9	5.3
30	1.1	5.4	0.8	0.4	0.8	3.3	1.0	0.7	1.0	0.6	1.0	7.5
31	1.1	0.8	0.8	0.4	0.9	1.1	1.0	0.9	1.0	0.6	1.0	1.3
32	0.9	3.5	0.8	> 10	0.7	7.5	0.9	4.4	1.0	5.5	1.0	5.3
33	0.8	3.5	0.8	1.3	0.8	7.5	1.1	0.6	1.1	0.5	1.0	5.4
34	0.9	1.4	0.8	2.2	0.8	7.6	0.8	3.3	1.1	0.6	1.0	6.4
35	0.8	3.4	0.7	1.5	0.8	5.3	1.0	0.8	1.2	0.8	0.9	5.9
36	1.1	0.5	0.8	5.1	1.0	1.1	1.2	0.4	1.3	0.5	1.0	0.7
37	0.8	1.8	0.7	5.5	0.8	2.4	1.1	0.5	1.1	1.2	0.8	2.0
38	0.9	5.7	0.6	5.2	0.9	3.8	0.9	4.4	1.0	4.2	0.8	3.9
39	1.5	0.6	0.8	4.3	1.1	1.1	1.5	1.0	1.4	1.2	1.1	0.6
40	1.0	0.8	0.9	0.7	0.9	6.8	1.2	0.7	1.2	1.6	1.0	5.7
41	1.0	0.8	0.8	1.0	0.9	6.1	1.1	2.2	1.2	1.9	1.0	6.2
42	1.0	2.2	0.7	7.1	1.0	5.9	1.0	0.7	1.1	1.6	1.1	1.6
43	1.0	0.8	0.6	8.2	0.9	5.7	1.1	0.7	1.1	1.7	1.1	4.4
44	1.0	0.8	0.8	0.7	0.9	6.6	1.1	0.7	1.2	1.6	1.0	1.7
45	1.0	0.8	0.7	0.7	0.9	6.6	1.1	0.7	1.2	1.6	1.0	7.4
46	1.0	1.8	0.8	4.2	0.9	1.3	1.2	2.2	1.4	1.3	1.2	1.7
47	1.0	0.5	0.8	5.0	0.9	3.9	1.2	2.1	1.4	1.3	1.1	2.8
48	1.0	5.4	0.8	1.9	0.9	4.2	1.2	2.2	1.3	2.1	1.2	2.2
49	1.0	1.1	0.8	2.0	0.9	4.5	1.2	2.2	1.3	2.2	1.1	2.1
50	1.0	1.8	0.8	1.9	0.9	1.2	1.3	2.3	1.2	1.7	1.1	2.2
51	1.0	1.1	0.7	> 10	0.9	3.1	1.1	2.2	1.2	2.2	1.1	4.5
52	1.0	5.4	0.8	1.0	1.0	4.0	1.1	2.2	1.2	1.7	1.2	5.1
53	1.0	5.4	0.7	1.2	1.0	3.5	1.1	2.2	1.2	1.7	1.1	2.2
54	1.0	0.9	0.7	2.4	1.0	4.5	1.2	2.3	1.2	1.7	1.1	4.5
55	1.0	0.6	0.7	2.1	1.0	3.4	1.1	2.4	1.2	2.1	1.2	4.1
56	1.1	1.0	0.8	0.7	1.0	3.2	1.1	2.3	1.3	1.3	1.2	3.9
57	1.0	3.3	0.7	3.8	1.0	3.3	1.1	0.7	1.1	3.9	1.1	4.9
58	1.1	5.7	0.7	5.0	0.9	1.6	1.3	2.0	1.2	0.9	1.0	3.8
59	1.1	3.0	0.8	1.8	1.0	2.4	1.2	2.0	1.2	0.7	1.1	5.9
60	1.3	2.3	0.8	5.3	1.1	1.7	1.3	1.2	1.5	0.7	1.3	1.0
61	1.2	0.3	0.8	5.1	1.3	0.9	1.4	0.5	1.5	0.4	1.5	0.5
62	1.4	0.4	0.8	6.4	1.2	0.9	1.6	0.4	1.7	0.3	1.4	0.4
63	1.3	0.4	0.8	4.7	1.3	0.9	1.6	0.5	1.7	0.4	1.4	0.4
64	1.4	0.4	0.8	6.5	1.3	0.9	1.4	0.5	1.5	0.4	1.6	0.4
65	1.2	0.3	0.7	6.2	1.4	1.0	1.4	0.5	1.5	0.4	1.5	0.5
66	1.2	0.4	0.8	6.0	1.4	1.0	1.4	0.5	1.5	0.4	1.5	0.4
67	1.2	0.4	0.8	5.2	1.4	0.9	1.4	0.5	1.5	0.4	1.5	0.4
68	1.2	0.4	0.8	5.6	1.3	0.9	1.4	0.5	1.5	0.4	1.4	0.5
69	0.9	1.0	0.7	> 10	0.7	5.2	0.8	7.2	0.9	6.4	0.9	6.3

Figure 3. Matrix of the alignment among the ligands and the reference templates.**Table 2.** Statistical Results of the MTA 3D-QSAR Model

Vars	PC	r ²	q ²	SDEP _{TS1}	SDEP _{TS2}
1594	1	0.86	0.66	0.73	0.67
1594	2	0.92	0.77	0.64	0.67
1594	3	0.94	0.77	0.70	0.68
1594	4	0.95	0.76	0.70	0.70
1594	5	0.97	0.74	0.68	0.71

ring, while the hydroxamate group favorably interacted with a' and b' regions.

Compound **63** (MMP3 IC₅₀ = 136 nM) is approximately 45-fold less active than **67**, and it differs in the absence of the phenylmethylsulfane group. As shown in Figure 6, the lack of the aromatic ring resulted in the lost of a crucial interaction with region D of the C3 probe, thereby explaining its lower MMP3 activity.

Compound **12** (MMP3 IC₅₀ = 20.0 nM) was only 6-fold less active than **67**, but it bore a unique structure. The *tert*-butyl acetate substituent favorably interacted with regions C and D of the C3 probe, and the methoxy group favorably

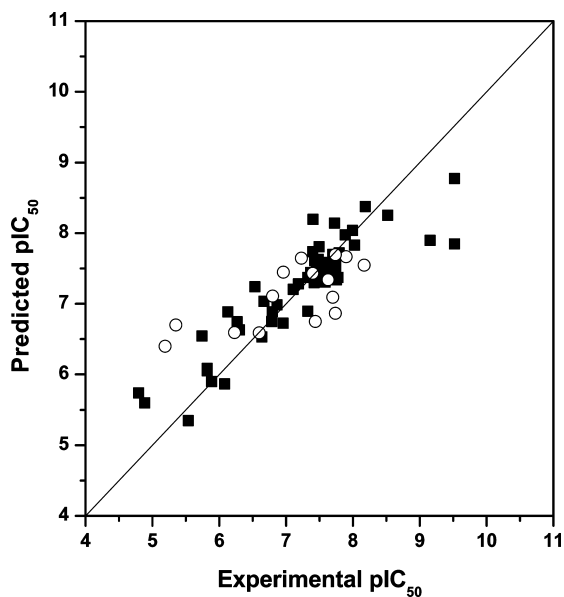


Figure 4. Plots of the 3D-QSAR model for MMP3. The training set is represented by (■) and the test set by (○).

Table 3. Statistical Results of the DBA 3D-QSAR Model⁹

Vars	PC	r ²	q ²	SDEP _{TS1}	SDEP _{TS2}
1177	1	0.68	0.55	0.83	0.78
1177	2	0.88	0.75	0.80	0.84
1177	3	0.91	0.77	0.79	0.85
1177	4	0.94	0.75	0.79	0.88
1177	5	0.97	0.73	0.82	0.88

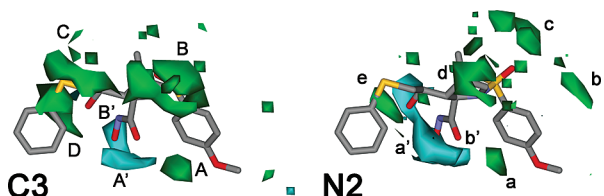


Figure 5. Negative (cyan) and positive (green) regions of the PLS coefficient plot obtained with the C3 and N2 probes. Compound 67 is also displayed as a reference structure.

interacted with region B. With regard to the N2 probe, the interaction with d and e again confirmed the importance of the lipophilic interaction of the *tert*-butyl acetate. Unlike for 67, the hydroxamic acid was unable to interact with the a' and b' regions.

Finally, compound 27 (MMP3 IC₅₀ = 2900 nM) was one of the least active inhibitors among those analyzed in the present study. As shown in Figure 6, the lack of lipophilic substituents bound in proximity of the hydroxamic acid eliminated all favorable interactions with the C3 probe, and the presence of a four-atom spacer between the hydroxamic acid and the carbonyl group resulted in a distortion of the position of the hydroxamate group, which subsequently lost the favorable interactions with the a' and b' regions of the N2 probe.

Since the alignment of the ligands was performed using reference ligands extracted from MMP3 X-ray structures, it became beneficial to check for consistencies between the MMP3 protein and the 3D-QSAR maps. In Figure 7, the binding site of MMP3 overlaps with the 3D PLS coefficient maps of the C3 and the N2 probes. For the C3 probe, region A was in the proximity of Pro238, supporting an important

role for this residue, already suggested in our recent studies.⁹ For the N2 probe, the electrostatic surface b' corresponded to Glu219, and the a region supported the role for Pro238.

A second validation of the 3D-QSAR model was carried out by taking into account the most important published MMP3 inhibitors tested with a fluorogenic assay. This is the same type of biological assay that was used for the compounds included in the training set and the first external test set. This assay consisted of measuring the fluorescent products formed by the cleavage of the substrate in the presence of different concentrations of the inhibitors.

A total of 106 MMP3 inhibitors were considered as part of the second external test set.^{41–44} As shown in Figure 8, these compounds can be schematically represented by three different scaffolds. Among them, only the general structure C was previously considered in the training set used for the 3D-QSAR model development.

As highlighted in Table 2 and in the Supporting Information, even if the predicted activity of 14 compounds differed from the experimental activity more than one logarithmic unit, the model was capable of predicting the activity of this large external test set, as the 3D-QSAR model was able to predict the activity of these compounds with an SDEP_{TS2} of 0.67. Furthermore, as reported in Table 3, the DBA 3D-QSAR model showed poorer predictive ability, as the SDEP of the external test set (SDEP_{TS2}) was 0.85 (see also Table S1 in the Supporting Information).

We recently reported the design, synthesis, and *in vitro* evaluation of a series of iminodiacetyl-based hydroxamate-benzenesulfonamide conjugates that strongly inhibit both MMPs and carbonic anhydrases, some in the nanomolar to subnanomolar range.⁴⁵ These compounds were tested for their inhibitory activity on several MMPs and TACE, and some of them were characterized by the presence of a 4-sulfamoylphenylethyl group (see Table 5), significantly different from those described for the 3D-QSAR model development. However, despite these structural differences, we decided to employ the 3D-QSAR model for predicting the MMP3 inhibitory activity of these compounds. Since the IC₅₀ values for some of these compounds were below 30 nM, their inhibitory activities were *in vitro* evaluated on MMP3. As shown in Table 5, compounds 3c, 6c, and 7 displayed nanomolar MMP3 activity, and the 3D-QSAR model provided a good predictive ability for these compounds, with a calculated SDEP value of 0.76. Once again the MTA model showed a better predictive ability with respect to the DBA 3D-QSAR model, as the latter provided for these compounds an SDEP of 0.94.

CONCLUSIONS

In this paper we tested the possibility of using a multi-template alignment method for the development of a 3D-QSAR model. This alignment is performed using a ligand-based procedure in which each ligand is aligned with all the available experimental templates, and those with the highest score alignment are selected for 3D-QSAR calculations. We recently reported docking-based 3D-QSAR models built to analyze MMP2 inhibitors. 3D-QSAR models for MMP2, MMP3, and MMP9 were developed, which allow for the prediction of the binding affinities of new MMP2 inhibitors and provide information about the selectivity of these inhibitors against MMP3 and MMP9. MMP3 is an important

Table 4. Actual versus Predicted Data of the MTA 3D-QSAR Model^a

The table displays chemical structures and corresponding experimental (Exp) and calculated (Calcd) pIC₅₀ values for various MMP3 inhibitors. Compounds are categorized by their chemical features, such as amide linkages, substituents (R groups), and specific functional groups like hydroxyl (OH), methoxymethyl (OMOM), and propargyl.

Cpd.	R	Exp ³¹	Calcd
1	H	6.96	7.45
2	Me	7.33	6.89
3	Et	7.44	7.34
4	n-Pr	7.43	7.61
5	i-Bu	7.11	7.20
6	Bn	7.72	7.60
7	2-Pyridylmethyl	7.80	7.72
8	3-Pyridylmethyl	7.48	7.63
9	4-Pyridylmethyl	7.40	7.74
10	Allyl	7.74	7.46
11	1-Naphthylmethyl	7.54	7.50
12	CH ₂ CO ₂ -t-Bu	7.70	7.70
13	OH	6.96	6.72
14	SPh	8.03	7.83

Cpd.	R ₁ , R ₂	Exp ³¹	Calcd
15	-CH ₃ , -OCH ₂ OCH ₂ CH ₃	7.59	7.31
16	-CH ₃ , -OCH ₂ OCH ₂ CH ₂ OCH ₃	7.42	7.30
17	-CH ₃ , -OCOC(CH ₃) ₃	7.19	7.28
18	-CH ₃ , -OH	7.44	6.75
19	-CH ₃ , -H	5.19	6.40
20	-CH ₂ CH ₃ , -OCH ₂ OCH ₂ CH ₃	7.54	7.42
21	-CH ₂ CH ₃ , -OCH ₂ OCH ₂ CH ₂ OCH ₃	7.49	7.34
22	-CH ₂ CH ₃ , -OCOC(CH ₃) ₃	7.40	7.43

Cpd.	R	Exp ³⁷	Calcd
23		6.08	5.86
24		4.80	5.74
25		4.89	5.60

Cpd.	R	Exp ³⁴	Calcd
26		5.74	6.54
27		5.54	5.34

Cpd.	R	Exp ³⁴	Calcd
28	-OH	5.89	5.90
29 ^a	-OBOM	6.13	6.89
30	-(CH ₂) ₂ Ph	6.80	6.89
31	-(CH ₂) ₃ Ph	6.60	6.59

Cpd.	R	Exp ³⁴	Calcd
32	-OH	5.82	6.08
33 ^b	-OMOM	5.82	6.05

Cpd.	R	Exp ³⁴	Calcd
34	-OH	6.27	6.74
35 ^b	-OMOM	6.64	6.53

Cpd.	R	Exp ³²	Calcd
51	methyl	7.41	8.19
52	methoxyethyl	7.70	7.09
53	cyclopropyl	7.63	7.34
54	propargyl	7.89	7.98
55	acetyl	7.64	7.58
56	mesyl	7.49	7.81

Cpd.	R	Exp ³⁵	Calcd
57	/	9.15	7.90

Cpd.	R	Exp ³⁵	Calcd
58	-i-But	6.67	7.04
59	-(CH ₂) ₂ Ph	6.23	6.59

Cpd.	R	Exp ³⁵	Calcd
60	/	6.79	6.75

Cpd.	R	Exp ³³	Calcd
61	CH ₃ SCH ₂ Ph	8.17	7.55
62	CHCH ₃	6.53	7.24
63	CH ₂ OH	6.87	6.98
64	CH ₂ SCH ₂ CH ₂ Ph	8.19	8.38
65	CH ₂ SCH ₂ PhOCH ₃	7.78	7.37
66	CH ₂ OCH ₂ Ph	8.00	8.04
67		8.52	8.25
68		7.73	8.14

Cpd.	R	Exp ³⁸	Calcd
69	/	7.33	7.37

^a The compounds reported in bold belong to the first external test set. A superscript a denotes BOM, benzyloxymethyl. A superscript b denotes MOM, methoxymethyl.

target for the treatment of arthritis, and furthermore numerous X-ray structures of MMP3 complexes have been published. Thus, in order to test the reliability of the MTA method, we chose MMP3 inhibition as a case study.

The data obtained through the MTA method highlighted a good internal and external predictive ability, which was confirmed by implementation of a second external test set of approximately one hundred MMP3 inhibitors. Finally,

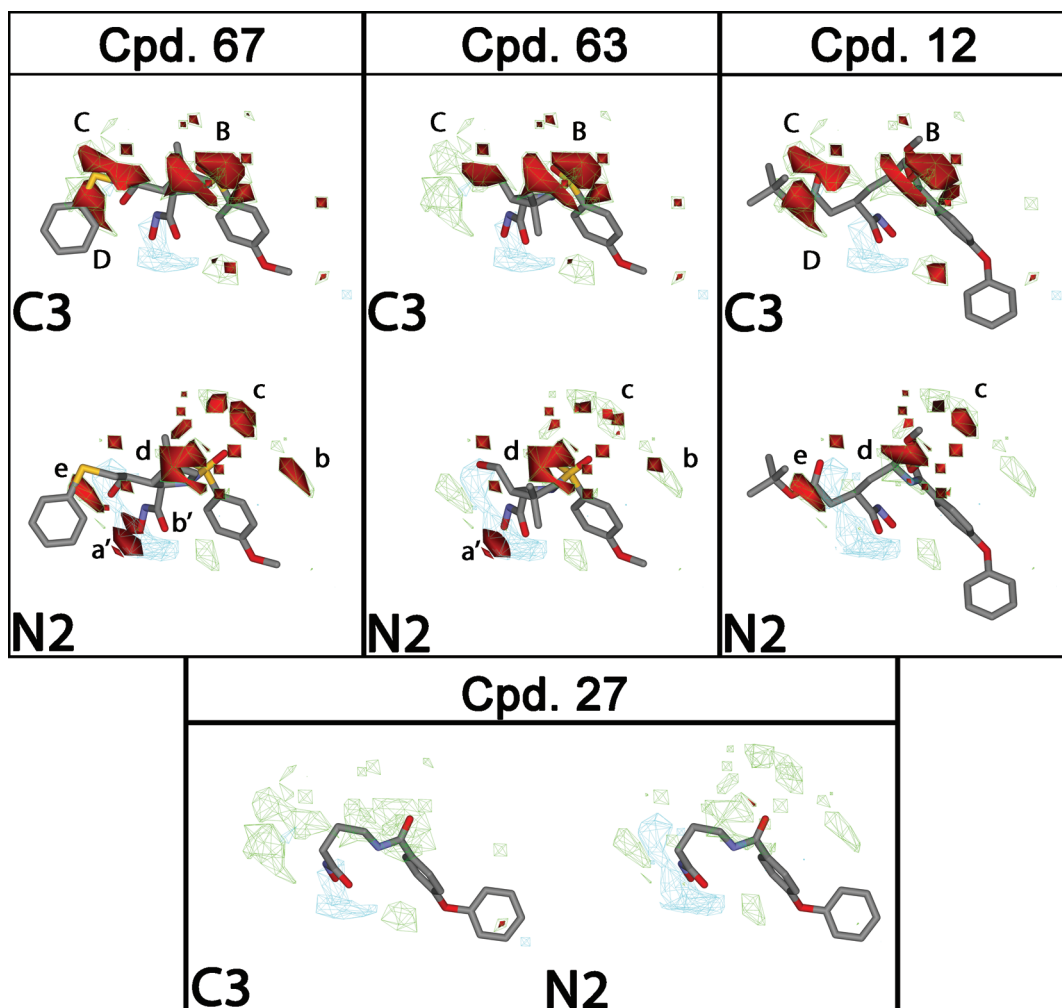


Figure 6. Positive activity contribution plots (red polyhedrons) for C3 and N2 probes of compounds **67**, **63**, **12**, and **27** embedded in the negative (cyan) and positive (green) regions of the PLS coefficient plot.

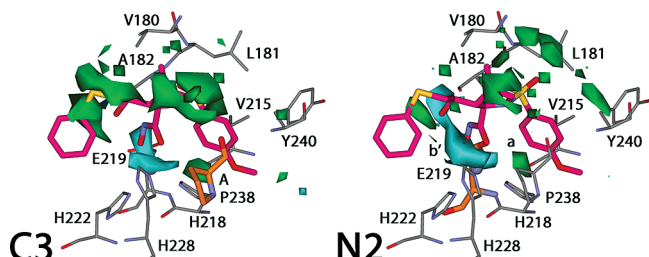


Figure 7. PLS coefficient plots obtained with the C3 and N2 probes superimposed on the MMP3 binding site. Compound **67** is also displayed as a reference structure.

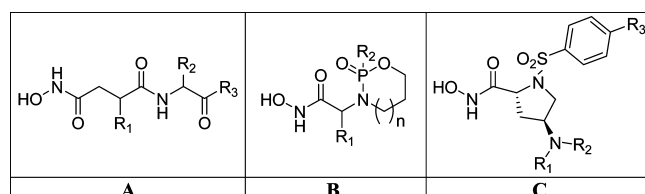


Figure 8. General scaffolds of the compounds of the second external test set.

since the 3D-QSAR model predicted some of the recently published iminodiacetyl based hydroxamate-benzenesulfonamide conjugates as being particularly active, we examined these compounds *in vitro* for their MMP3 activity. Gratifyingly, some displayed low nanomolar activity, suggesting

Table 5. Activity Data for Compounds **1**, **2**, **3a-3c**, **6a-6c**, and **7** for MMP3 Inhibition

Cpd.	\bar{R}_1	\bar{R}_2	\bar{R}_3	IC ₅₀ (nM)	
				Exp.	Pred.
1	H	-SO ₂ PhOCH ₃	OH	1380	125.9
2	H	-SO ₂ PhOPh	OH	37.2 ± 0.2	49.4
3a	i-Pr	-SO ₂ PhOCH ₃	OH	182 ± 31	60.3
3b	i-Pr	-SO ₂ PhPh	OH	127 ± 11.5	88.9
3c	i-Pr	-SO ₂ PhOPh	OH	6.7 ± 1	37.1
6a	H	-SO ₂ PhOCH ₃	NH-SPE	140 ± 12	30.1
6b	H	-SO ₂ PhPh	NH-SPE	430 ± 23	34.8
6c	H	-SO ₂ PhOPh	NH-SPE	6.1 ± 0.4	19.7
7	i-Pr	-SO ₂ PhOPh	NH-SPE	1.2 ± 0.15	18.3
SDEP				0.76	

that the overall model was reliable and could be applied toward the design of new active MMP3 inhibitors.

Comparison of the data obtained through the MTA method with that obtained by means of the DBA method highlighted that they possessed the same internal predictive ability, but the MTA 3D-QSAR model clearly showed a better external predictive ability, as it showed a lower value of SDEP for all three reported external test sets.

In all, our results indicated that the use of a large number of templates derived from X-ray structures for aligning ligands could improve the quality of 3D-QSAR models.

EXPERIMENTAL SECTION

X-ray Reference Structures. The X-ray structure of the nine MMP3-inhibitor complexes were obtained from the Protein Data Bank¹⁹ and then aligned. 1B3D was used as a reference structure, and the backbone of the proteins was considered for the alignment. MMP3 seemed to possess a low degree of movement upon the binding of different ligands, since the rmsd of the protein backbone never exceeded the value of 0.4 Å. The alignment of the complexes, carried out using the backbone of the proteins, determined an “indirect” alignment of the nine ligands that was based on their interactions with the proteins. Maintaining this alignment, the ligands were extracted. Bonds and hydrogen atoms of the ligands were added by Maestro 8.0⁴⁶.

Alignment of the Molecules. A total of 184 MMP3 inhibitors, tested using fluorimetric assays quantified using peptido-mimetic substrates, were retrieved from literature. All compounds were built by means of Maestro 8.0⁴⁶ and were then minimized by means of Macromodel⁴⁷ using the Conjugate Gradient method and MMFFs force field until a convergence value of 0.05 kcal/Å•mol was reached. The alignment of the compounds was developed using the ROCS 2.2 software,³⁹ which is a shape-similarity method based on the Tanimoto-like overlap of volumes. The alignment was developed using the Combo score, which combines the Tanimoto shape score with the color score that added the score for the appropriate overlap of groups with similar properties (donor, acceptor, hydrophobe, cation, anion, and ring). All other parameters were used as their ROCS default values. The maximum number of conformations per molecule was 1000, generated using OMEGA 2.1.0.⁴⁸

Compounds were aligned to all nine X-ray reference structures previously extracted, and for each compound for the studies described, we considered only the alignments in which the rmsd between the ZBG of the ligand and that of the X-ray reference structure was below 1.2 Å. Among these conformations, the one with the best Combo score was chosen (see Figure 3). For the ligands that did not display at least one rmsd between the ZBG of the ligand and that of the X-ray reference structure below 1.2 Å, the conformation with the lower rmsd was chosen.

3D-QSAR Model. The GOLPE program⁴⁰ was used to define a 3D-QSAR model, using GRID interaction fields⁴⁹ as descriptors. The training set and test sets already used for the development of the docking-based 3D-QSAR study were employed.⁹ For the second test set, we used 106 MMP3 inhibitors retrieved from the literature. Interaction energies between the selected probes and each molecule were calculated using a grid spacing of 1 Å. A combination of C3 (corresponding to a methyl group) and N2 (corresponding to neutral flat NH₂) was used.

Variable selection was carried out by zeroing values with absolute values below 0.06 kcal/mol and removing variables with a standard deviation below 0.1. Additionally, variables which either exhibited only two values or had a skewed distribution were also removed. The smart region definition algorithm⁵⁰ was applied with 10% of the active variables as

the seed number (selected in the PLS weight space), using a critical distance cutoff of 2.5 Å, and a collapsing distance cutoff of 4.0 Å. The groups were then used in the Fractional Factorial Design.

As reported in Table 4, compounds **24**, **49**, and **57** in the training set gave a poor prediction. It could make sense to consider these three compounds as outliers; however, we maintained them in the training set because otherwise we could not compare the MTA 3D QSAR results with those obtained using the DBA approach in which all the compounds were considered.

Biological Methods: MMP Inhibition Assays. Recombinant human pro-MMP3 was purchased from Calbiochem. Proenzyme was activated immediately prior to use with 5 µg/mL trypsin for 30 min at 37 °C followed by 62 µg/mL soybean trypsin inhibitor (SBTI).⁵¹

For assay measurements, the inhibitor stock solutions (100 mM DMSO) were further diluted, at 7 different concentrations (ranging from 0.01 nM to 300 µM) in the fluorometric assay buffer (FAB: Tris 50 mM, pH = 7.5, NaCl 150 mM, CaCl₂ 10 mM, 0.05% Brij 35 and 1% DMSO). Activated enzyme (final concentration 5 nM) and inhibitor solutions were incubated in the assay buffer for 4 h at 25 °C. After the addition of 200 µM solution of the fluorogenic substrate Mcu-Arg-Pro-Lys-Pro-Val-Glu-Nva-Trp-Arg-Lys(Dnp)-NH₂ (Sigma) in DMSO (final concentration 2 µM), the hydrolysis was monitored every 15 s for 20 min recording the increase in fluorescence ($\lambda_{\text{ex}} = 328 \text{ nm}$, $\lambda_{\text{em}} = 393 \text{ nm}$) using a SpectraMax Gemini XS plate reader from Molecular Devices. The assays were performed in triplicate in a total volume of 200 µL per well in 96-well microtiter plates (Corning, black, NBS). Control wells lacked inhibitor. The MMP inhibition activity was expressed in relative fluorescent units (RFU). Percent of inhibition was calculated from control reactions without the inhibitor. IC₅₀ values were determined using the formula $V_i/V_o = 1/(1 + [I]/IC_{50})$, where V_i is the initial velocity of substrate cleavage in the presence of the inhibitor at concentration [I] and V_o is the initial velocity in the absence of the inhibitor. Results were analyzed using SoftMax Pro software⁵² and GraFit software.⁵³

ACKNOWLEDGMENT

Financial support was provided by Fondazione Monte dei Paschi di Siena (“Strumenti terapeutici innovativi per la modulazione dell’attività di metalloproteasi della matrice implicate nelle patologie tumorali cerebrali”), which is gratefully acknowledged. Many thanks are due to Prof. Gabriele Cruciani and Prof. Sergio Clementi (Molecular Discovery and MIA srl) for the use of the GOLPE program in their chemometric laboratory (University of Perugia, Italy) and for having provided the GRID program.

Supporting Information Available: Actual versus predicted data for the second external test set (Table S1). This material is available free of charge via the Internet at <http://pubs.acs.org>.

REFERENCES AND NOTES

- (1) Tervo, A. J.; Nyrönen, T. H.; Rönkkö, T.; Poso, A. Comparing the Quality and Predictiveness Between 3D QSAR Models Obtained from Manual and Automated Alignment. *J. Chem. Inf. Comput. Sci.* **2004**, 44, 807–816.

- (2) Pandey, G.; Saxena, A. K. 3D QSAR Studies on Protein Tyrosine Phosphatase 1B Inhibitors: Comparison of the Quality and Predictivity among 3D QSAR Models Obtained from Different Conformer-Based Alignments. *J. Chem. Inf. Model.* **2006**, *46*, 2579–2590.
- (3) Kaur, K.; Talele, T. T. Structure-Based COMFA and COMSIA Study of Indolinone Inhibitors of PDK1. *J. Comput.-Aided Mol. Des.* **2009**, *23*, 25–36.
- (4) Park, H. Y.; Ju, S. M.; Lee, D. Y.; Zhang, H.; Kim, C. K. 3D-QSAR Studies on DATAs and DAPYs for HIV-RT Inhibitors Using CoMFA and COMSIA Approaches. *QSAR Comb. Sci.* **2009**, *28*, 218–225.
- (5) Zhou, Z.; Madura, J. D. CoMFA 3D-QSAR Analysis of HIV-1 RT Nonnucleoside Inhibitors, TIBO Derivatives Based on Docking Conformation and Alignment. *J. Chem. Inf. Comput. Sci.* **2004**, *44*, 2167–2178.
- (6) Matter, H.; Will, D. W.; Nazaré, M.; Schreuder, H.; Laux, V.; Wehner, V. Structural Requirements for Factor Xa Inhibition by 3-Oxybenzamides with Neutral P1 Substituents: Combining X-ray Crystallography, 3D-QSAR, and Tailored Scoring Functions. *J. Med. Chem.* **2005**, *48*, 3290–3312.
- (7) Tuccinardi, T.; Nuti, E.; Ortore, G.; Supuran, C. T.; Rossello, A.; Martinelli, A. Analysis of Human Carbonic Anhydrase II: Docking Reliability and Receptor-Based 3D-QSAR Study. *J. Chem. Inf. Model.* **2007**, *47*, 515–525.
- (8) Durdagi, S.; Papadopoulos, M. G.; Papahatjis, D. P.; Mavromoustakos, T. Combined 3D QSAR and Molecular Docking Studies to Reveal Novel Cannabinoid Ligands with Optimum Binding Activity. *Bioorg. Med. Chem. Lett.* **2007**, *17*, 6754–6763.
- (9) Tuccinardi, T.; Nuti, E.; Ortore, G.; Rossello, A.; Avramova, S. I.; Martinelli, A. Development of a Receptor-Based 3D-QSAR Study for the Analysis of MMP2, MMP3, and MMP9 Inhibitors. *Bioorg. Med. Chem.* **2008**, *16*, 7749–7758.
- (10) Tintori, C.; Magnani, M.; Schenone, S.; Botta, M. Docking, 3D-QSAR Studies and *in Silico* ADME Prediction on c-Src Tyrosine Kinase Inhibitors. *Eur. J. Med. Chem.* **2009**, *44*, 990–1000.
- (11) La Motta, C.; Sartini, S.; Tuccinardi, T.; Nerini, E.; Da Settimo, F.; Martinelli, A. Computational Studies of Epidermal Growth Factor Receptor: Docking Reliability, Three-Dimensional Quantitative Structure-Activity Relationship Analysis, and Virtual Screening Studies. *J. Med. Chem.* **2009**, *52*, 964–975.
- (12) Tuccinardi, T.; Calderone, V.; Rapposelli, S.; Martinelli, A. Proposal of a New Binding Orientation for Non-Peptide AT1 Antagonists: Homology Modeling, Docking and Three-Dimensional Quantitative Structure-Activity Relationship Analysis. *J. Med. Chem.* **2006**, *49*, 4305–4316.
- (13) Tuccinardi, T.; Ortore, G.; Rossello, A.; Supuran, C. T.; Martinelli, A. Homology Modeling and Receptor-Based 3D-QSAR Study of Carbonic Anhydrase IX. *J. Chem. Inf. Model.* **2007**, *47*, 2253–2262.
- (14) Narkhede, S. S.; Degani, M. S. Pharmacophore Refinement and 3D-QSAR Studies of Histamine H₃ Antagonists. *QSAR Comb. Sci.* **2007**, *26*, 744–753.
- (15) Long, W.; Liu, P.; Li, Q.; Xu, Y.; Gao, J. 3D-QSAR Studies on a Class of IKK-2 Inhibitors with GALAHAD Used to Develop Molecular Alignment Models. *QSAR Comb. Sci.* **2008**, *27*, 1113–1119.
- (16) Ryu, C. K.; Lee, Y.; Park, S. G.; You, H. J.; Lee, R. Y.; Lee, S. Y.; Choi, S. 3D-QSAR Studies of Heterocyclic Quinones with Inhibitory Activity on Vascular Smooth Muscle Cell Proliferation Using Pharmacophore-Based Alignment. *Bioorg. Med. Chem.* **2008**, *16*, 9772–9779.
- (17) Boström, J.; Böhm, M.; Gundertorffte, K.; Klebe, G. A 3D QSAR Study on a Set of Dopamine D4 Receptor Antagonists. *J. Chem. Inf. Comput. Sci.* **2003**, *43*, 1020–1027.
- (18) Fan, F.; Zhu, J.; Ni, S.; Cheng, J.; Tang, Y.; Kang, C.; Li, J.; Jiang, H. Refinement and 3D-QSAR Studies of Inhibitors of Cyclophilin A Containing Amide Linker. *QSAR Comb. Sci.* **2009**, *28*, 183–193.
- (19) Berman, H. M.; Westbrook, J.; Feng, Z.; Gilliland, G.; Bhat, T. N.; Weissig, H.; Shindyalov, I. N.; Bourne, P. E. The Protein Data Bank. *Nucleic Acids Res.* **2000**, *28*, 235–242.
- (20) Okada, Y.; Shinmei, M.; Tanaka, O.; Naka, K.; Kimura, A.; Nakanishi, I.; Bayliss, M. T.; Iwata, K.; Nagase, H. Localization of Matrix Metalloproteinase 3 (Stromelysin) in Osteoarthritic Cartilage and Synovium. *Lab. Invest.* **1992**, *66*, 680–690.
- (21) Chapman, K. T.; Durette, P. L.; Caldwell, C. G.; Sperow, K. M.; Niedzwiecki, L. M.; Harrison, R. K.; Saphos, C.; Christen, A. J.; Olszewski, J. M.; Moore, V. L.; MacCoss, M.; Hagmann, W. K. Orally Active Inhibitors of Stromelysin-1 (MMP-3). *Bioorg. Med. Chem. Lett.* **1996**, *6*, 803–806.
- (22) Chen, L.; Rydel, T. J.; Gu, F.; Dunaway, C. M.; Pikul, S.; Dunham, K. M.; Barnett, B. L. Crystal Structure of the Stromelysin Catalytic Domain at 2.0 Å Resolution: Inhibitor-Induced Conformational Changes. *J. Mol. Biol.* **1999**, *293*, 545–557.
- (23) Pikul, S.; McDow Dunham, K. L.; Almstead, N. G.; De, B.; Natusch, M. G.; Anastasio, M. V.; McPhail, S. J.; Snider, C. E.; Taiwo, Y. O.; Rydel, T.; Dunaway, C. M.; Gu, F.; Mieling, G. E. Discovery of Potent, Achiral Matrix Metalloproteinase Inhibitors. *J. Med. Chem.* **1998**, *41*, 3568–3571.
- (24) Cheng, M.; De, B.; Almstead, N. G.; Pikul, S.; Dowty, M. E.; Dietsch, C. R.; Dunaway, C. M.; Gu, F.; Hsieh, L. C.; Janusz, M. J.; Taiwo, Y. O.; Natusch, M. G.; Hudlicky, T.; Mandel, M. Design, Synthesis, and Biological Evaluation of Matrix Metalloproteinase Inhibitors Derived from a Modified Proline Scaffold. *J. Med. Chem.* **1999**, *42*, 5426–5436.
- (25) Pikul, S.; Dunham, K. M.; Almstead, N. G.; De, B.; Natusch, M. G.; Taiwo, Y. O.; Williams, L. E.; Hynd, B. A.; Hsieh, L. C.; Janusz, M. J.; Gu, F.; Mieling, G. E. Heterocycle-Based MMP Inhibitors with P2' Substituents. *Bioorg. Med. Chem. Lett.* **2001**, *11*, 1009–1013.
- (26) Natusch, M. G.; Cheng, M.; Wahl, C. T.; Pikul, S.; Almstead, N. G.; Bradley, R. S.; Taiwo, Y. O.; Mieling, G. E.; Dunaway, C. M.; Snider, C. E.; McIver, J. M.; Barnett, B. L.; McPhail, S. J.; Anastasio, M. B.; De, B. Design and Synthesis of Conformationally-Constrained MMP Inhibitors. *Bioorg. Med. Chem. Lett.* **1998**, *8*, 2077–2080.
- (27) Almstead, N. G.; Bradley, R. S.; Pikul, S.; De, B.; Natusch, M. G.; Taiwo, Y. O.; Gu, F.; Williams, L. E.; Hynd, B. A.; Janusz, M. J.; Dunaway, C. M.; Mieling, G. E. Design, Synthesis, and Biological Evaluation of Potent Thiazine- and Thiazepine-Based Matrix Metalloproteinase Inhibitors. *J. Med. Chem.* **1999**, *42*, 4547–4562.
- (28) Cheng, M.; De, B.; Pikul, S.; Almstead, N. G.; Natusch, M. G.; Anastasio, M. V.; McPhail, S. J.; Snider, C. E.; Taiwo, Y. O.; Chen, L.; Dunaway, C. M.; Gu, F.; Dowty, M. E.; Mieling, G. E.; Janusz, M. J.; Wang-Weigand, S. Design and Synthesis of Piperazine-Based Matrix Metalloproteinase Inhibitors. *J. Med. Chem.* **2000**, *43*, 369–380.
- (29) Natusch, M. G.; Bookland, R. G.; De, B.; Almstead, N. G.; Pikul, S. Development of New Hydroxamate Matrix Metalloproteinase Inhibitors Derived from Functionalized 4-Aminoprolines. *J. Med. Chem.* **2000**, *43*, 4948–4963.
- (30) Kohno, T.; Hochigai, H.; Yamashita, E.; Tsukihara, T.; Kanaoka, M. Crystal Structures of the Catalytic Domain of Human Stromelysin-1 (MMP-3) and Collagenase-3 (MMP-13) with a Hydroxamic Acid Inhibitor SM-25453. *Biochem. Biophys. Res. Commun.* **2006**, *344*, 315–322.
- (31) Yamamoto, S.; Nakatani, S.; Ikura, M.; Sugiura, T.; Nishita, Y.; Itadani, S.; Ogawa, K.; Ohno, H.; Takahashi, K.; Nakai, H.; Toda, M. Design and Synthesis of an Orally Active Matrix Metalloproteinase Inhibitor. *Bioorg. Med. Chem.* **2006**, *14*, 6383–6403.
- (32) Becker, D. P.; Villamil, C. I.; Barta, T. E.; Bedell, L. J.; Boehm, T. L.; Decrescenzo, G. A.; Freskos, J. N.; Getman, D. P.; Hockerman, S.; Heintz, R.; Howard, S. C.; Li, M. H.; McDonald, J. J.; Caron, C. P.; Funckes-Shippy, C. L.; Mehta, P. P.; Munie, G. E.; Swearingen, C. A. Synthesis and Structure-Activity Relationships of Beta- and Alpha-Piperidine Sulfone Hydroxamic Acid Matrix Metalloproteinase Inhibitors with Oral Antitumor Efficacy. *J. Med. Chem.* **2005**, *48*, 6713–6730.
- (33) Hanessian, S.; MacKay, D. B.; Moitessier, N. Design and Synthesis of Matrix Metalloproteinase Inhibitors Guided by Molecular Modeling. Picking the S(1) Pocket Using Conformationally Constrained Inhibitors. *J. Med. Chem.* **2001**, *44*, 3074–3082.
- (34) Nakatani, S.; Ikura, M.; Yamamoto, S.; Nishita, Y.; Itadani, S.; Habashita, H.; Sugiura, T.; Ogawa, K.; Ohno, H.; Takahashi, K.; Nakai, H.; Toda, M. Design and Synthesis of Novel Metalloproteinase Inhibitors. *Bioorg. Med. Chem.* **2006**, *14*, 5402–5422.
- (35) Hanessian, S.; Moitessier, N.; Cantin, L. D. Design and Synthesis of MMP Inhibitors using N-Arylsulfonylaziridine Hydroxamic Acids as Constrained Scaffolds. *Tetrahedron* **2001**, *57*, 6885–6900.
- (36) Rossello, A.; Nuti, E.; Carelli, P.; Orlandini, E.; Macchia, M.; Nencetti, S.; Zandomeneghi, M.; Balzano, F.; Uccello Barretta, G.; Albini, A.; Benelli, R.; Cercignani, G.; Murphy, G.; Balsamo, A. N-i-Propoxy-N-biphenylsulfonylaminobutylhydroxamic Acids as Potent and Selective Inhibitors of MMP-2 and MT1-MMP. *Bioorg. Med. Chem. Lett.* **2005**, *15*, 1321–1326.
- (37) Ikura, M.; Nakatani, S.; Yamamoto, S.; Habashita, H.; Sugiura, T.; Takahashi, K.; Ogawa, K.; Ohno, H.; Nakai, H.; Toda, M. Discovery of a New Chemical Lead for a Matrix Metalloproteinase Inhibitor. *Bioorg. Med. Chem.* **2006**, *14*, 4241–4252.
- (38) Chollet, A. M.; Le Diguarher, T.; Murray, L.; Bertrand, M.; Tucker, G. C.; Sabatini, M.; Pierre, A.; Atassi, G.; Bonnet, J.; Casara, P. General Synthesis of Alpha-Substituted 3-Bisaryloxy Propionic Acid Derivatives as Specific MMP Inhibitors. *Bioorg. Med. Chem. Lett.* **2001**, *11*, 295–299.
- (39) Rush, T. S.; Grant, J. A.; Mosyak, L.; Nicholls, A. A Shape-Based 3-D Scaffold Hopping Method and its Application to a Bacterial Protein-Protein Interaction. *J. Med. Chem.* **2005**, *48*, 1489–1495.
- (40) GOLPE, version 4.5; Multivariate Infometric Analysis Srl.: Viale dei Castagni 16, Perugia, Italy, 1999.
- (41) Marcq, V.; Mirand, C.; Decarme, M.; Emonard, H.; Hornebeck, W. MMPs Inhibitors: New Succinylhydroxamates with Selective Inhibition

- of MMP-2 Over MMP-3. *Bioorg. Med. Chem. Lett.* **2003**, *13*, 2843–2846.
- (42) Sørensen, M. D.; Blaehr, L. K.; Christensen, M. K.; Høyter, T.; Latini, S.; Hjarnaa, P. J.; Björkling, F. Cyclic Phosphinamides and Phosphonamides, Novel Series of Potent Matrix Metalloproteinase Inhibitors with Antitumour Activity. *Bioorg. Med. Chem.* **2003**, *11*, 5461–5484.
- (43) Fray, M. J.; Burslem, M. F.; Dickinson, R. P. Selectivity of Inhibition of Matrix Metalloproteases MMP-3 and MMP-2 by Succinyl Hydroxamates and their Carboxylic Acid Analogues Is Dependent on P3' Group Chirality. *Bioorg. Med. Chem. Lett.* **2001**, *11*, 567–570.
- (44) Natchus, M. G.; Bookland, R. G.; De, B.; Almstead, N. G.; Pikul, S.; Janusz, M. J.; Heitmeyer, S. A.; Hookfin, E. B.; Hsieh, L. C.; Dowty, M. E.; Dietsch, C. R.; Patel, V. S.; Garver, S. M.; Gu, F.; Pokross, M. E.; Mieling, G. E.; Baker, T. R.; Foltz, D. J.; Peng, S. X.; Bornes, D. M.; Strojnowski, M. J.; Taiwo, Y. O. Development of New Hydroxamate Matrix Metalloproteinase Inhibitors Derived from Functionalized 4-Aminoprolines. *J. Med. Chem.* **2000**, *43*, 4948–4963.
- (45) Marques, S. M.; Nuti, E.; Rossello, A.; Supuran, C. T.; Tuccinardi, T.; Martinelli, A.; Santos, M. A. Dual Inhibitors of Matrix Metalloproteinases and Carbonic Anhydrases: Iminodiacetyl-Based Hydroxamate-Benzenesulfonamide Conjugates. *J. Med. Chem.* **2008**, *51*, 7968–7979.
- (46) *Maestro*, version 8.0; Schrödinger Inc.: Portland, OR, 2007.
- (47) *Macromodel*, version 8.5; Schrödinger Inc.: Portland, OR, 2001.
- (48) Boström, J.; Greenwood, J. R.; Gottfries, J. Assessing the Performance of OMEGA with Respect to Retrieving Bioactive Conformations. *J. Mol. Graphics Modell.* **2003**, *21*, 449–462.
- (49) *GRID*, version 22a; Molecular Discovery Ltd.: West Way House, Elms Parade, Oxford, U.K., 2004.
- (50) Pastor, M.; Cruciani, G.; Clementi, S. Smart Region Definition: a New Way to Improve the Predictive Ability and Interpretability of Three-Dimensional Quantitative Structure-Activity Relationships. *J. Med. Chem.* **1997**, *40*, 1455–1464.
- (51) Knight, C. G.; Willenbrock, F.; Murphy, G. A Novel Coumarin-Labelled Peptide for Sensitive Continuous Assays of the Matrix Metalloproteinases. *FEBS Lett.* **1992**, *296*, 263–266.
- (52) *SoftMax Pro*, version 4.7.1; Molecular Devices: Sunnyvale, CA, 2006.
- (53) *GraFit*, version 4; Erithacus Software Ltd.: Surrey, UK, 2004.

CI900118V